Journal of Colloid and Interface Science 694 (2025) 137664

Contents lists available at ScienceDirect

Journal of Colloid And Interface Science

journal homepage: www.elsevier.com/locate/jcis

Short Communication

# Composition-dependent tunability of the cell interactions of hybrid lipid – block copolymer vesicles

Juan Martinez [a,b], Nicola Ingram [b], Nikil Kapur [c], David G. Jayne [b,d], Paul A. Beales [a,*]

[a] School of Chemistry and Astbury Centre for Structural Molecular Biology, University of Leeds, Leeds, West Yorkshire LS2 9JT, UK
[b] Leeds Institute for Medical Research, University of Leeds, Leeds, West Yorkshire LS9 7TF, UK
[c] School of Mechanical Engineering, University of Leeds, Leeds, West Yorkshire LS2 9JT, UK
[d] The John Goligher Colorectal Surgery Unit, St. James's University Hospital, Leeds Teaching Hospital Trust, Beckett Street, Leeds, West Yorkshire LS9 7TF, UK

## GRAPHICAL ABSTRACT

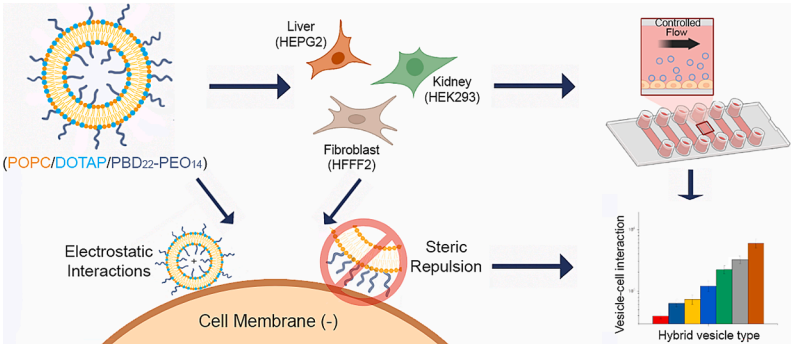


## ARTICLE INFO

*Keywords:*
Phospholipids
Polybutadiene-*block*-polyethylene oxide
Cell uptake
Flow cytometry
Nanomedicine
Drug delivery

## ABSTRACT

Hybrid vesicles composed of phospholipids and block copolymers are of interest for a wide range of applications due to the broad tunability of their material properties that can synergistically combine desirable properties of liposomes and polymersomes. A major application of vesicles in biotechnology has been in the field of drug delivery, where understanding and controlling vesicle interactions with cells is of vital importance. Here, we investigate the tunability of hybrid vesicle interaction with three distinct cell lines through modulating non-specific interactions. We formulate vesicles composed of three different constituents, the zwitterionic lipid 1-palmitoyl-2-oleoyl-*glycero*-3-phosphocholine (POPC), the cationic lipid 1,2-dioleoyl-3-trimethylammonium-propane (DOTAP) and the amphiphilic diblock copolymer Poly(1,2-butadiene)-*b*-poly(ethylene oxide) ($PBD_{22}$-$PEO_{14}$). This enables the tunability of cell interactions through electrostatic attraction to anionic cellular membranes and steric repulsion from the polymeric PEO brush layer. We establish a microfluidic flow protocol to enhance the reproducibility of vesicle-cell interactions by controlling the hydrodynamic stresses during incubation and washing steps. We demonstrate a high degree of tunability of cell interactions and low cytotoxicity across the three cell lines investigated (HFFF2, HEK293, HepG2). These initial findings offer critical insights into the engineering of hybrid vesicles and their potential applications in drug delivery.

* Corresponding author.
*E-mail address:* p.a.beales@leeds.ac.uk (P.A. Beales).

https://doi.org/10.1016/j.jcis.2025.137664
Received 22 February 2025; Received in revised form 8 April 2025; Accepted 20 April 2025
Available online 21 April 2025

## 1. Introduction

Vesicles such as liposomes and polymersomes have been extensively studied for drug encapsulation and controlled release [1–3]. Their usability spans multiple fields, including food, cosmetics, and medicine [4]. Due to their design versatility and biocompatibility, they offer a promising alternative to conventional therapies [5]. A recent example of the capabilities of these technologies is their use in mRNA-based vaccines against SARS-CoV-2 [6].

In nanomedicine, understanding the non-specific interactions between vesicles and cells is crucial. These interactions are influenced primarily by the surface charge and the presence of steric polymers on the vesicle surface. Cationic liposomes, which possess a positive surface charge, have been widely studied for their enhanced cellular uptake due to electrostatic attraction to the negatively charged cellular membrane. Studies have shown that cationic liposomes exhibit higher internalisation rates compared to their neutral or anionic counterparts [7,8]. However, there is a consensus that cationic liposomes may induce cell death or an inflammatory response [9,10]. The balance between efficient uptake and cytotoxicity remains a significant challenge, as excessive positive charge can disrupt cellular membranes and lead to toxicity [11].

Surface modification with polyethylene glycol (PEG) is a common strategy to improve vesicle stability and reduce non-specific interactions. PEGylation creates "stealth" vesicles that evade the immune system, prolonging circulation time and reducing clearance [12,13]. PEG chains provide a steric barrier that prevents opsonisation and subsequent phagocytosis by the mononuclear phagocyte system, thus enhancing the vesicle's half-life in the bloodstream [14]. However, PEGylation also introduces steric hindrance, which can inhibit the effective interaction of vesicles with target cells, potentially reducing therapeutic efficacy [15,16]. Furthermore, there is now evidence that patients can develop PEG-specific antibodies from repeat doses of PEGylated nanomedicines, potentially reducing their efficacy [17].

Hybrid lipid-polymer vesicles combine the beneficial properties of both liposomes and polymersomes, offering enhanced stability, controlled release, and improved biocompatibility [18–20]. These hybrid systems are particularly promising in nanomedicine due to their ability to fine-tune the physicochemical properties for specific therapeutic applications. Several studies have investigated the formulation of hybrid vesicles for drug delivery and controlled release [21–26]. Similar to other vesicle types, hybrid vesicles can interact with and be internalised by cells [27–31]. In particular, hybrid vesicles have been shown to enhance the efficacy of targeted delivery [32]. Hybrid vesicles can be engineered to achieve a synergistic effect, whereby the lipid component provides biocompatibility, and the polymer component offers mechanical strength and stability [19].

Here, we investigate the cell interaction of hybrid vesicles composed of a mixture of neutral phospholipid (POPC), a cationic lipid (DOTAP) and a diblock copolymer ($PBD_{22}$-$PEO_{14}$). Unsaturated phospholipids, which are fluid at ambient and physiological temperatures (such as POPC and DOTAP), are known to form well-mixed membranes with PBD-PEO copolymers [33–36], such that our formulations are expected to form homogeneous mixed membranes without large heterogeneities or domains formed by phase separation of the amphiphilic components. The block copolymer enhances the elasticity and toughness of the membrane, making the vesicles more resilient to sterilisation and preservation processes required for biomedical formulations [37]. Furthermore, the block copolymer provides a PEG corona to the vesicles for steric stabilisation to reduce opsonisation *in vivo* [38]. The cationic DOTAP enhances interaction with anionic cell membranes, facilitating cell uptake [39]. Finally the POPC acts to dilute the surface PEG density and enhance fluidity of the vesicle membrane, further enabling the physical properties and cell interactions of these nanoparticles to be tuned.

This study focuses on the interactions of hybrid lipid-polymer vesicles with three cell lines representing distinct biological contexts: human foetal foreskin fibroblasts (HFFFs), as a model for normal primary cells; human embryonic kidney cells (HEK293); and hepatocellular carcinoma cells (HepG2), due to their well-characterised properties [29,40,41]. We aim to compare the cellular uptake and cytotoxicity of these hybrid vesicles with cationic liposomes of similar charge content. By comparing the non-specific interactions of these vesicles with cells when subjected to precisely regulated flow conditions, we hope to gain insights into optimising their design for therapeutic applications. This microfluidics-enabled approach enables us to understand how incorporating cationic lipids and PEGylation from the block copolymer regulates the balance between enhanced cellular uptake and potential cytotoxicity, thereby guiding the development of more effective and safer nanomedicine delivery systems.

## 2. Results

### 2.1. Microfluidic flow parameters for enhanced reproducibility of experimental conditions

To standardise hybrid vesicle-cell interaction studies, we employed microfluidic flow channels (Ibidi μ-Slide $VI^{0.4}$), allowing precise control over flow rate, incubation time, and volume. Conventional nanoparticle washing methods risk introducing variability in shear stress, which can lead to inconsistencies between samples. Although this study does not directly quantify the variability between methods, the microfluidic system was prioritised to mitigate the inherent limitations of manual washing through standardisation of parameters (Fig. 1A). By maintaining a tightly controlled flow environment, this approach is expected to reduce experiment-to-experiment variability in shear stress, suggesting methodological advantages over traditional techniques.

Wide ranges of fluid shear stresses are experienced within the body. This can vary from 0.05 to 0.76 $Nm^{-2}$ in the veins and 0.3 to 0.7 $Nm^{-2}$ in peripheral arteries, which are the most common delivery routes for vesicle-based technologies [42]. However, cell uptake of nanomedicines is expected to predominately occur in the lower shear stress environments of local tissues, where the interstitial fluid flow leads to shear stresses that decrease below 0.1 $Nm^{-2}$ [43,44]. The shear stress ($\tau$, $Nm^{-2}$) in the microfluidic channels can be calculated using the manufacturer-supplied formula, $\tau = 176.1\eta\phi$, where $\eta$ is the dynamical viscosity of the fluid ($Nsm^{-2}$) and $\phi$ is the fluid flow rate in $mLmin^{-1}$ [45]. Therefore, for cell culture media with $\eta \approx 7.2 \times 10^{-4}$ $Nsm^{-2}$ at 37 °C, the shear stresses of interstitial fluid flow in tissues are equivalent to fluid flow rates up to 0.79 mL $min^{-1}$.

To initially screen and determine our flow and incubation parameters, we investigated two vesicle compositions that we anticipated to provide the maximum and minimum cell interactions based upon our three selected amphiphiles: the zwitterionic lipid 1-palmitoyl-2-oleoyl-*glycero*-3-phosphocholine (POPC), the cationic lipid 1,2-dioleoyl-3-trimethylammonium-propane (DOTAP) and the amphiphilic diblock copolymer Poly(1,2-butadiene)-*b*-poly(ethylene oxide) ($PBD_{22}$-$PEO_{14}$). These vesicles were composed of 100 % DOTAP liposomes (positive control), due to strong electrostatic interactions with the cell membrane, and 100 % $PBD_{22}$-$PEO_{14}$ polymersomes (negative control), due to the steric repulsion provided by the dense PEO (a synonym of PEG) brush layer. All vesicles were labelled with 0.5 mol% 1,2-dioleoyl-*sn-glycero*-3-phosphoethanolamine-N-(lissamine rhodamine B sulfonyl) (ammonium salt) (Rh-DOPE), a phospholipid-based fluorophore, enabling consistent tracking across formulations. Following the interaction between vesicles and cells, the fluorescence intensity from the Rh-DOPE probe coincident with the cells was analysed using confocal fluorescence microscopy. These initial experiments were conducted using HFFF2 cells.

To investigate the effect of flow rate on vesicle removal, vesicles were initially incubated with cells under standard growth conditions for 4 h. Following this incubation period, unbound vesicles were washed

using a total volume of 500 μL, applied at flow rates ranging from 50 to 1000 μL $min^{-1}$ (Fig. 1B). This method ensured that the total wash volume remained constant (500 μL) across all tested flow rates while the duration of washing varied proportionally with the selected rate (for example, 10 min at 50 μL $min^{-1}$ compared to 0.5 min at 1000 μL $min^{-1}$). As expected, DOTAP liposomes show significantly higher cell interaction than $PBD_{22}$-$PEO_{14}$ polymersomes, validating that this technique can differentiate between the cell interactions of different vesicle formulations. The fluorescence intensity of the HFFF2 cells decreased with increasing flow rate for both vesicle compositions, plateauing above 650 μL $min^{-1}$, demonstrating the removal of some weakly-bound vesicles on the cell surface at higher flow rates. This demonstrates the value of creating reproducible flow rates for washing the cells prior to imaging in order to achieve reproducible and comparable data. Notably, the proportional decrease in fluorescence intensity for both vesicle formulations was roughly parallel across the flow rate range investigated such that the ratio between these fluorescence intensities was found to be independent of flow rate (Supplementary Fig. 1). Since higher flow rates were also seen to remove weakly-adherent cells from the microchannel, a relatively low flow rate of 100 μL.$min^{-1}$ was chosen for further studies.

Next, we optimised the incubation time from adding the vesicle formulations to the HFFF2 cells to the flow-driven washing step prior to imaging (Fig. 1C). At a fixed volume flow rate of 100 μL $min^{-1}$ and washing volume of 500 μL, we observe an increase in the fluorescence intensity of the cells with increasing incubation time for both vesicle formulations. The increase in cell uptake with incubation time is greatest for the DOTAP liposomes. The increase in cell uptake for both formulations is greatest within the first 4 h, after which the fluorescence intensity of the cells begins to saturate. The continued growth and

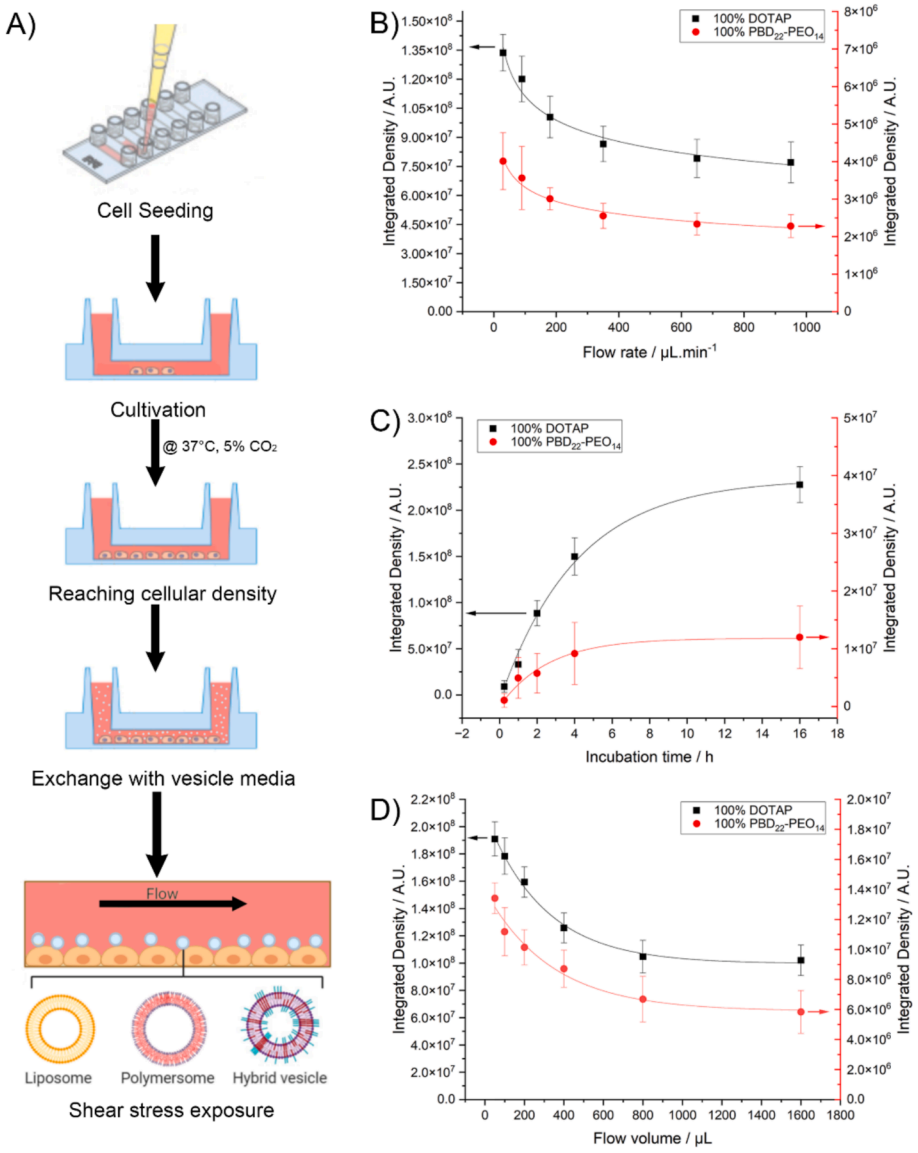


**Fig. 1. Determining conditions for the study of vesicle-cell interactions in microfluidic channels.** A) Schematic representation of the protocol followed to set up the parameters for the flow experiments. After seeding cells and reaching confluency in the Ibidi μ-Slide $VI^{0.4}$, the media was exchanged for vesicle media and incubated (37 °C, 5 % $CO_2$). After incubation, unbound and weakly bound vesicles were washed under controlled flow conditions that exposed the cells to reproducible fluid shear stresses. B) Integrated density (IntDen) of the cell-associated vesicles (4 h incubation) after washing with 500 μL at different flow rates. Higher flow rates reduce residual vesicle binding, reflecting shear-dependent removal efficiency. C) IntDen of the cell-associated vesicles after incubation at different times (37 °C, 5 % $CO_2$) followed by washing with 500 μL PBS at 100 μL $min^{-1}$ (5 min duration). D) IntDen of the cell-associated vesicles after being washed with increasing PBS volumes at 100 μL $min^{-1}$ post 4 h incubation. The vesicles were labelled using 0.5 mol% Rh-DOPE, which enabled the cell interactions to be quantified using ImageJ. IntDen reflects the cumulative fluorescence across the image, measured as the total fluorescence per representative area, in arbitrary units (A.U.).

division of the cells, which will eventually reach and surpass a cell surface density of full confluence, also complicates the use of longer incubation times. Therefore, an incubation time of 4 h was set for further experiments.

Finally, we determined a fixed flow volume for washing the cells. These experiments were conducted at a fixed incubation time of 4 h and flow rate of 100 μLmin$^{-1}$, varying the washing volume between 50 and 1600 μL (Fig. 1D). Increased total flow volumes up to approximately 800 μL decreased the fluorescence intensity of cells for both formulations as unbound and weakly bound vesicles are removed from the microchannel. However, larger washing volumes were seen to lead to detachment of some of the HFFF2 cells meaning that a compromise was required between removal of excess vesicles without significant loss of cells. Therefore, a washing volume of 500 μL was chosen for further experiments as this is close to the point at which the fluorescence intensity plateaus, ensuring good removal of excess vesicles. Note that the volume of the microchannel is approximately 30 μL, hence this represents a washing volume ~ 17x that of the channel's capacity.

### 2.2. Composition-dependent interactions of hybrid vesicles with HFFF2 cells

A range of vesicle compositions were investigated for their interactions with HFFF2 cells using our fixed experimental parameters of a 4 h incubation time and a washing volume of 500 μL at a flow rate of 100 μL min$^{-1}$. Fig. 2A displays some example confocal microscopy images of cells interacting with each vesicle type studied. The nucleus of these cells was labelled with DAPI (blue) and the cellular membranes were labelled with Wheat germ agglutinin (WGA) Alexa fluor 488 conjugate (green). Finally, the vesicles were labelled with 0.5 mol% Rh-DOPE (red), as above.

The interaction of the vesicle formulations with HFFF2 cells was quantified by the red fluorescence inside these cells (Fig. 2B). Among the single-component vesicles, POPC liposomes exhibited an intermediate level of cell interaction between DOTAP liposomes and $PBD_{22}$-$PEO_{14}$ polymersomes. The interaction of multicomponent hybrid vesicles could be rationally tuned between those of the pure components. Specifically, 50/50 POPC/ $PBD_{22}$-$PEO_{14}$ hybrid vesicles showed relatively low cell uptake, with fluorescence intensity falling between that of $PBD_{22}$-$PEO_{14}$ polymersomes and POPC liposomes. Incorporation of DOTAP into hybrid vesicles (50/50 DOTAP/ $PBD_{22}$-$PEO_{14}$) significantly increased cell uptake compared to POPC liposomes ($p < 0.01$) but remained lower than DOTAP liposomes. Further modulation was observed with 25/25/50 DOTAP/POPC/$PBD_{22}$-$PEO_{14}$ hybrid vesicles, which exhibited lower uptake than 50/50 DOTAP/ $PBD_{22}$-$PEO_{14}$ ($p < 0.05$) but remained significantly higher than POPC liposomes. Statistical analysis using one-way ANOVA followed by Dunnett's test confirmed significant differences between the groups, with comparisons made relative to 100% DOTAP liposomes as the highest binding reference. These results demonstrate that hybrid vesicles containing cationic lipids offer a highly

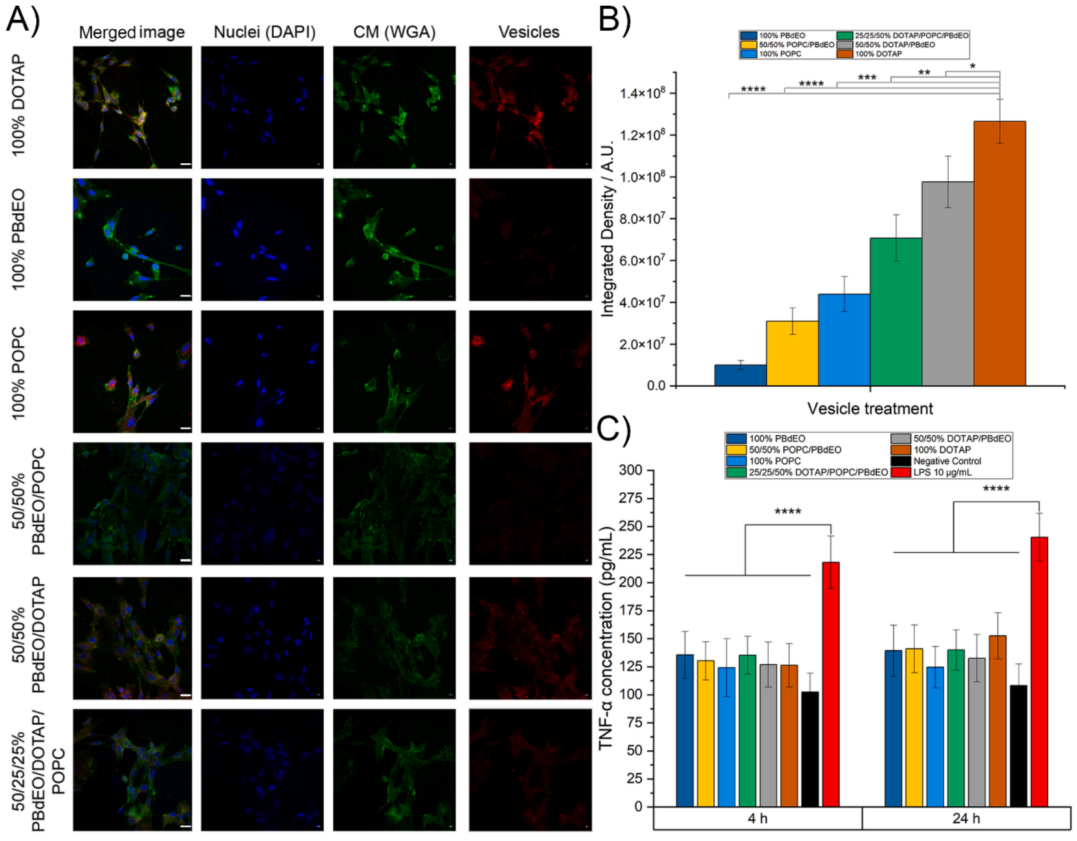


**Fig. 2. Hybrid vesicle affinity to and inflammatory stimulation of HFFF2 cells.** A) Confocal pictures (scale bar 12.5 μm, magnification 400X) of the cells after 1 h incubation on ice with the vesicles and 4 h incubation at 37 °C, 5 % $CO_2$. Cell nuclei were stained with DAPI (blue); cellular membranes were stained with WGA (green); vesicle fluorescence signal labelled with Rh-DOPE (red). B) Fluorescence intensity of hybrid vesicle formulations following interaction with HFFF2 cells using our microfluidic protocol. Vesicle formulations were incubated with cells for 4 h at 37 °C with 5 % $CO_2$. Cells were then washed with 500 μL of PBS at a flow rate of 100 μL min$^{-1}$ ($\tau = 0.013$ Nsm$^{-2}$). C) TNF-α concentrations from cellular supernatants after different exposure times to the vesicle formulations. TNF-α concentration in pg/mL produced by the HFFF2 cells after 4 and 24 h exposure time to the different vesicle compositions at 37 °C with 5 % $CO_2$. The negative control represents HFFF2 cells that were grown solely with regular DMEM growth media. 10 μg/mL of LPS acts as a positive inflammatory control for the analysis of the inflammatory response of the cells. One-way ANOVA followed by post-hoc Dunnett's test were used for analysis. * Represents a statistically significant difference, $p < 0.05$; **** represents a statistically significant difference with $p < 0.0001$. (For interpretation of the references to colour in this figure legend, the reader is referred to the web version of this article.)

tunable system for modulating cell interaction.

To assess whether any of these vesicle formulations stimulated a significant inflammatory response in the HFFF2 cells, we conducted ELISA assays to measure the production of the pro-inflammatory cytokine TNF-α (Fig. 2C). After exposure to 100 μM initial vesicle solutions (diluted in serum-free DMEM), which was subsequently washed for microfluidic experiments. All formulations exhibited a similar ~ 20 % increase in TNF-α production compared to untreated cells. However, this was within error as it was not found to be statistically significant at either the 4 h or 24 h time points. The TNF-α produced in response to the vesicle formulations was also much lower than positive control of HFFF2 cells stimulated by 10 μg $mL^{-1}$ of *E. coli* lipopolysaccharide (LPS). Therefore, we conclude that these vesicle formulations do not stimulate a significant inflammatory response at the concentration studied.

### 2.3. Flow cytometry demonstrates a consistent hierarchy of vesicle affinities for a range of cell lines

To verify our data with a complementary, high-throughput, quantitative approach, we employed flow cytometry to investigate vesicle interactions with HFFF2 cells and two further cell lines, human embryonic kidney cells (HEK293) and a human epithelial liver cancer cell line (Hep G2). Fig. 3A illustrates the gating strategy used to identify and select relevant cell detection events accurately. The process began with the identification of cells based on forward and side scatter area (FSC-A vs SSC-A), enabling the exclusion of debris and non-cellular particles. To ensure the analysis focused only on single cells, the gated population was further refined using FSC-A vs forward scatter height (FSC-H) to isolate singlets and remove aggregates. The singlet population was then examined for wheat germ agglutinin (WGA-A) expression, plotted against count to distinguish WGA+ cells from WGA− cells. Finally, the WGA+ population was analysed for rhodamine fluorescence intensity, represented as a histogram, from which the median fluorescence intensity (MFI) was extracted for quantitative analysis. These results confirm the trend of vesicle affinities for HFFF2 cells found using our microfluidic cell imaging strategy (Fig. 3B). Notably, the same trends in cell affinity for the different formulations were also observed for two very different cell lines, Hep G2 (Fig. 3C) and HEK293 (Fig. 3D). This is consistent with the non-specific nature of the vesicle-cell interactions (a combination of electrostatic attraction and steric repulsion). However, the data also hints at differences in affinity with the same vesicle composition across different cell lines, where the median fluorescent intensity varies between cell lines for a given vesicle type. This latter observation hints at the possibility of some element of cell-specific targeting despite the vesicle-cell interactions being non-specific in nature. This may, for instance, be partially driven by differences in the anionic surface charge of the membrane and different cell uptake efficiencies for each cell type. Still, we also anticipate that additional, complex interactions must be at play in determining the overall affinity for different vesicle compositions with the cells.

## 3. Discussion

Our study elucidates the critical role of vesicle composition in modulating cellular interactions. By investigating the cell-affinity of vesicles composed of cationic (DOTAP), neutral lipid (POPC), and polymeric ($PBD_{22}$-$PEO_{14}$) components, we aimed to understand how each component contributes to cellular adherence and uptake. Through flow cytometry MFI measurements and zeta potential characterisation (Supplementary Table S1), we established a quantitative correlation between cationic charge density (DOTAP content) and cellular uptake across all cell lines (Fig. 2B, 3B-D), suggesting that surface charge quantitatively controls internalisation. This strong electrostatic affinity aligns with findings in other vesicle studies, which indicate that cationic vesicles exhibit stronger cell adhesion due to their attraction to negatively charged cell membrane components, such as phosphatidylserine (PS) and glycosaminoglycans (GAGs) [46–49]. The selection of low melting temperature ($T_m$) lipids (POPC: $T_m$ = -2 °C; DOTAP: $T_m$ = -10 °C) ensured membrane fluidity at physiological temperatures, which is critical for consistent cellular interactions. While lipid phase behaviour near $T_m$ can unpredictably alter uptake kinetics [50,51], our vesicles avoid this complication, enabling the clear interpretation of charge- and steric-dependent effects.

In contrast, as expected, neutral vesicles such as POPC and $PBD_{22}$-$PEO_{14}$ showed low adherence to cell lines under all tested conditions due to the absence of electrostatic interactions with the negatively charged cell membranes. Notably, our findings suggest that DOTAP-containing vesicles had significantly higher adherence, up to seven times greater than neutral vesicles, under specific conditions, demonstrating the impact of vesicle composition on cellular affinity. Modulating cellular interactions via vesicle composition offers a valuable mechanism for tailoring nanomedicine pharmacokinetics and biodistribution [2,52].

Compared to other hybrid systems, our $PBD_{22}$-$PEO_{14}$/phospholipid vesicles exhibit superior charge tunability to PEG-PLA/lipid hybrids [53], which show ≈ -29 to -35 mV zeta-potential modulation. In contrast, our DOTAP incorporation achieves a tunable range of greater than 45 mV (Supplementary Table S1). Unlike cholesterol-containing hybrids that prioritise membrane stability [54], our system's focus on charge-steric balance enables finer control of cellular interactions with cell-uptake controlled by DOTAP and block copolymer composition.

The use of a lipid-based probe, Rh-DOPE, as a universal fluorescent marker in all vesicle formulations may warrant careful interpretation, particularly for the purely polymeric 100 % $PBD_{22}$-$PEO_{14}$ vesicles. As demonstrated by Nam *et al.* [33], Rh-DOPE preferentially partitions into fluid polymer-rich domains that coexist with ordered lipid phases in hybrid membranes. Furthermore, these block copolymers are fully miscible with fluid phase phospholipids across the full compositional paramater space [35,36]. Therefore this probe is readily incorporated into and evenly dispersed within polymeric vesicles. However, once taken up by cells, fluorescent lipids and block copolymers may be trafficked to different sub-cellular locations due to their different structures. However, in this work, we only consider extent of cell uptake and not downstream trafficking of individual nanoparticle components within the cell.

Our experiments optimised parameters, such as washing volume, nanoparticle incubation time, and washing flow rate, to consistently study vesicle-cell interactions across vesicle types. Even in hybrid vesicles incorporating neutral polymers, the presence of cationic DOTAP maintained superior cellular adherence, supporting previous findings that indicate vesicles with cationic lipids can enhance cell interaction while reducing rapid clearance *in vivo* [55–57]. DLS results confirmed monomodal vesicle sizes, independent of composition, consistent with spherical nanoparticles with average diameters ≈110-125 nm (Supplementary Table S1). This consistency in size ensures that observed uptake differences reflect composition-dependent effects rather than size-based changes.

Incorporating DOTAP enhanced cellular adherence without inducing significant inflammatory responses, as measured by TNF-α production after 4 and 24 h of exposure (Fig. 2C). At the tested concentration (100 μM), all formulations maintained TNF-α levels statistically indistinguishable from those of untreated controls ($p > 0.5$), confirming a wide biocompatibility window. This is supported by the fact that PBS washing reduced residual vesicle concentrations to less than 100 μM, which is well below the cytotoxic thresholds tested. These results align with studies showing that cationic vesicles, when adequately balanced with neutral lipids like POPC, achieve strong cell membrane interactions with minimal inflammatory impact [58–60]. This effect is particularly evident in our hybrid vesicle (25/25/50 DOTAP/POPC/$PBD_{22}$-$PEO_{14}$), which showed comparable TNF-α levels to pure POPC liposomes despite their 27.2 mV zeta-potential (Supplementary Table S1). This demonstrates that compositional tuning can decouple cellular uptake from cytotoxicity - a critical consideration for therapeutic applications.

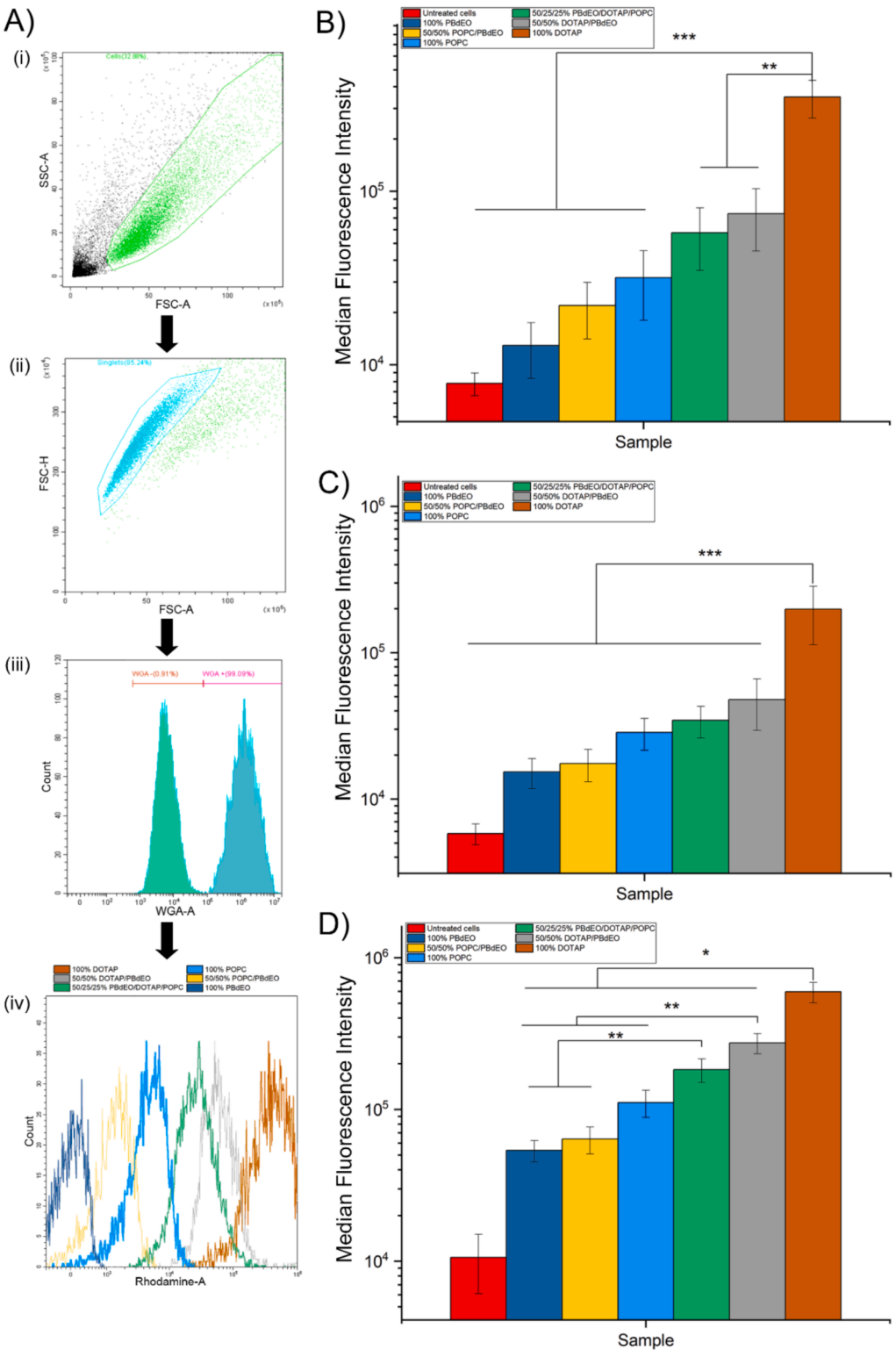


**Fig. 3. Flow cytometry confirms the relative affinity of different vesicle compositions to cells.** A) Example of the overall process for analysing samples to measure the cellular uptake of the hybrid vesicles tested using flow cytometry. After incubating the vesicles with the cells, a cellular solution ($1x10^6$ cells/mL) was loaded into the flow cytometer. (i) An initial gate was applied using forward scatter area (FSC-A) against side scatter area (SSC-A) to localise the cellular population. (ii) The gated cells were then plotted using FSC-A against forward scatter height (FSC-H) to eliminate any doublets and isolate the singlet population. Next (iii), the singlet population was illustrated using a histogram of the wheat germ agglutinin (WGA) response against the count; two examples are displayed in the figure. The left-most histogram corresponds to the fluorescent signal from cells alone (WGA-), while the one on the right of that is the fluorescent signal from cells treated with WGA only (WGA+ ). The flow cytometer was configured to record 10,000 events within the final gate (WGA+ vs count) and to plot the fluorescence histogram for the Rh-DOPE fluorescence in each recorded event. Median fluorescence intensity (MFI) is shown for B) HFFF2, C) HEPG2, and D) HEK293 cell lines following treatment with Rh-DOPE-labelled vesicles. The MFI is proportional to the concentration of vesicles within the cells. One-way ANOVA followed by post-hoc Tukey's test were used for analysis. *, **, *** Represents a statistically significant difference, $p < 0.05$, $p \leq 0.01$ and $p < 0.001$ respectively.

Interestingly, despite the neutral charge of POPC and $PBD_{22}$-$PEO_{14}$ vesicles, POPC exhibited higher intracellular localisation than $PBD_{22}$-$PEO_{14}$. This phenomenon could be attributed to the structural similarities between these phospholipid-based vesicles and cellular membranes, facilitating cell recognition and internalisation [61,62]. The presence of polymeric components, like $PBD_{22}$-$PEO_{14}$, can increase membrane thickness and introduce steric hindrance, possibly reducing cellular affinity. Such steric effects from polymer layers have been investigated by Le Meins et al. 2011 [50], showing that PEO from the polymer plays a key role in surface density, creating a physical barrier which prevents membrane interaction.

Our findings underscore the importance of vesicle composition and physical properties in determining cellular affinity. These findings contribute to the rational design of hybrid vesicle nanocarriers that can be tuned for specific interaction with target cells, advancing the development of vesicles for biomedical applications.

## 4. Conclusion

This study systematically explored how vesicle composition influences cellular uptake and inflammatory response across three different cell lines. Our findings demonstrate that cationic lipid incorporation (DOTAP) significantly enhances cellular affinity compared to purely polymeric $PBD_{22}$-$PEO_{14}$ vesicles while maintaining favourable biocompatibility profiles, as evidenced by TNF-α measurements. The quantitative correlations between DOTAP content and cellular uptake validated through flow cytometry provide formulators with a predictable framework for tuning vesicle-cell interactions. By carefully balancing POPC content, we achieved simultaneous optimisation of cellular uptake and inflammatory response, with hybrid vesicles showing minimal cytokine production despite their cationic character.

For translational applications, these findings offer critical design principles. First, the relationship between DOTAP concentration and cellular internalisation enables improved control over biodistribution without complex surface modifications. Second, the microfluidic washing protocol establishes standardised conditions for evaluating vesicle-cell interactions, addressing a key reproducibility challenge in nanomedicine development. Most importantly, the demonstrated ability to decouple cellular uptake from cytotoxicity through compositional tuning represents a significant advance toward clinically viable hybrid vesicle systems. These insights collectively provide a roadmap for engineering next-generation nanocarriers with tailored biological performance.

## 5. Materials and methods

### 5.1. Reagents

Poly(1,2-butadiene)-*b*-poly (ethylene oxide) ($PBD_{22}$-$PEO_{14}$) was purchased from Polymer Source., Inc. (Montreal, Quebec, Canada). 1-palmitoyl-2-oleoyl-*glycero*-3-phosphocholine (POPC), 1,2-dioleoyl-*sn-glycero*-3-phosphoethanolamine (Rh-DOPE), 1,2-dioleoyl-3-trimethylammonium-propane (DOTAP), and 100 nm polycarbonate membranes were purchased from Avanti Polar Lipids Inc. (Alabaster, Alabama, USA). HEPES buffer, NaCl, Sodium Citrate Dihydrate, Citric Acid, Sephadex G-50, Foetal Bovine Serum (FBS) and *E. coli* lipopolysaccharide (LPS) were purchased from Sigma-Aldrich Co. (Gillingham, Dorset, UK). Dulbecco's Modified Eagle Medium (DMEM), Dulbecco's Phosphate-Buffered Saline (DPBS) and 0.5 % Trypsin-EDTA (10x) were purchase from Gibco. (Loughborough, Leicestershire, England). Wheat germ agglutinin (WGA) Alexa fluor 488 conjugate and, ProLong Gold Antifade with DAPI were purchased from Thermo Fisher (California, USA). The human TNF-α quantikine ELISA kit was purchased from R&D systems (Minneapolis, USA). Human foetal foreskin fibroblast, 86,031,405 was purchased from European Collection of Authenticated Cell Cultures (ECACC) (Salisbury, UK). Human embryonic kidney 293 (HEK293), CRL-1573, and Human hepatoma G2 (HEPG2), HB-8065, were purchased from American Type Culture Collection (Manassas, USA).

### 5.2. Preparation of large unillamellar vesicles (LUVs)

LUVs were prepared using the thin film hydration and extrusion method. Briefly, 0.01183 g of $PBD_{22}$-$PEO_{14}$ was dissolved in 1 mL of chloroform (6.57 mM) with 42 μL of Rh-DOPE (0.5 mol%) for tracking during size exclusion column chromatography. The $PBD_{22}$-$PEO_{14}$ stock was mixed with POPC (Avanti Polar Lipids Inc.) and 0.5 mol% Rh-DOPE to prepare hybrid vesicles. The pure DOTAP, POPC, $PBD_{22}$-$PEO_{14}$ and hybrid vesicle mixtures were dried overnight in a vacuum desiccator to form a thin film. The film was rehydrated using 120 mM HEPES buffer pH 7.4 until no chunks of the film were visible using a vortex mixer; the vesicle solutions were frozen and thawed five times using liquid nitrogen and warm water and, finally, they were extruded to 100 nm using an extruder (LiposoFast, Avestin). The resulting vesicles were characterised for size and zeta potential using the zetasizer nano ZSP (Malvern analytical); these results are provided in the supplementary information (Table S1).

### 5.3. Establishment of cell lines

All cell lines were grown in DMEM 4.5 g/L glucose supplemented with 10 % FCS at 37 °C, 5 % $CO_2$ in a humidified incubator. Cells were trypsinised and counted using a Countess II FL Automated Cell. The Ibidi μ-Slide VI $^{0.4}$ (Fig. 1A) channels were seeded using a cellular concentration of $3x10^5$ cells/mL as recommended by the manufacturer, first by quickly pipetting 30 μL of the cells into each of the six channels. The cells were incubated for 1 h at 37 °C with 5 % $CO_2$ to allow attachment of the cells to the surface of the slide. After 1 h, 60 μL of DMEM medium was added to each reservoir of the slides and the slides were returned to the incubator for 48 h.

### 5.4. Tuning of flow parameters

The Ibidi μ-slides provide an adequate system to control the flow rates and the sheer stress during experiments; the vesicle-cell interaction is reported at different flow rates, washing volumes, and incubation times. 48 h after seeding, the cells reached 95 % confluence. The reservoir medium of the slides was discarded and replaced with 120 μL of 100 μM 100 % DOTAP liposomes or 120 μL of 100 μM $PBD_{22}$-$PEO_{14}$ (positive control and negative control) diluted in DMEM media (without FCS) and incubated at 37 °C with 5 % $CO_2$ for 4 h unless otherwise stated for the study (Fig. 1A shows a schematic representation of this protocol). Three different parameters were independently tested to study the affinity of vesicles to the cells: the washing flow rate, incubation time, and washing volume using a syringe mounted on an Aladdin-2000 pump (AL-2000) connected to the μ-slides via tubing. The flow rates inside the body vary; because of this, the shear stress used allow a close approximation of the flow conditions *in vivo*. Shear stress is the frictional force generated by a fluid flow in the microfluidic slides (units: $N/m^2$) [63]. Ibidi provides the conversion from flow rates to shear stress in the slides [45] using the formula:

$$\tau = 176.1\eta\phi$$

where $\Phi$ = flow rate mL/min, $\tau$=shear stress $Nm^{-2}$, and η = dynamical viscosity $Ns/m^2$ ($7.2x10^{-4}$ $Ns/m^2$ for DMEM media).

The human body possesses a wide range of shear stresses: this can vary from 0.05 to 0.76 $Nm^{-2}$ in the veins and 0.3 to 0.7 $Nm^{-2}$ in peripheral arteries, which are the most common delivery routes for vesicle-based technologies [42]. However, these shear stresses start to decrease below 0.1 $Nm^{-2}$ when reaching the interstitial flow of tissues [43,44]. Applying the Ibidi conversion formula to this shear stress results in a

flow rate of 1.2 mL $min^{-1}$. Knowing this flow rate to be equivalent to an *in vivo* setting, flow rates below 1 mL $min^{-1}$ were assessed. The incubation time of vesicles with the cells was tested. For this, the cells were incubated with vesicles for increasing amounts of time followed by washing with 500 μL of sterile PBS at a flow rate of 100 μL $min^{-1}$. The final parameter tested was the washing volume for which, after 4 h incubation with the vesicles, the cells were washed with 50, 100, 200, 400, 800, and 1600 μL of sterile PBS. After washing all the channels, the slides were visualised under an EVOS FL Cell Imaging System microscope. First the cells were located using a 10x objective (50 % lamp intensity with a phase contrast of 4/10); once the cells were located, the red fluorescent protein (RFP) filter was applied to visualise the fluorescence from the vesicles (if any) on the cells. The images were taken with a lamp intensity of 40 % and 120 ms exposure.

### 5.5. Analysis of Vesicle-Cell interactions

The previous parameters were used to assess the adhesive properties of different vesicles (Supplementary Table S1). After the HFFF2s had formed a monolayer for 48 h, the media from the reservoir was exchanged with 600 μL of 100 μM vesicle solution diluted in serum-free DMEM media and incubated at 37 °C with 5 % $CO_2$ for the chosen incubation time. Afterwards, the slides were attached via tubing to a syringe driver to dispense PBS volumes at different flow rates. The slides were visualised using an EVOS FL Cell Imaging System microscope, and the images were analysed with Fiji/ImageJ software. In ImageJ, the scale was calibrated using the scale bar from one of the images through the "Analyse" > "Set Scale" option. Background subtraction was performed by combining the negative control image (containing only cells) and the "Rolling Ball" method [64]. The test image (containing vesicles) and the negative control image were loaded to the Fiji/ImageJ software, and the negative control image was subtracted from the test image using the "Image Calculator" under the "Process" menu. Following this, a "Rolling Ball" background subtraction was applied with an 80-pixel radius by selecting "Process" > "Subtract Background". This approach effectively removed background noise while preserving key details. The "Integrated Density" was set as measurements in Fiji/ImageJ, and these values were obtained by pressing CTRL + M or selecting "Analyse" > "Measure." The integrated density measures the total fluorescence signals in an image, accounting for both the intensity and the analysis area. Finally, the data was exported as a Microsoft Excel spreadsheet and analysed and plotted using OriginPro 8.

### 5.6. Confocal microscopy

Glass coverslips were placed inside each well of a 6-well plate. Each well was seeded with HFFFs at a $3x10^5$ cells/mL concentration. After 24 h incubation, the plate was cooled down at 4 °C using an icebox; the media was exchanged with 3 mL of 100 μM vesicle solutions diluted in DMEM media (without FCS). The plate was incubated at 4 °C on ice for 1 h. The ice-cold incubation roughly gives all the vesicles the same start place due to the nonspecific inhibition of endocytosis (Chang, Wu, & Yuan, 2014). After the ice-cold incubation, the cells were incubated for 4 h at 37 °C with 5 % $CO_2$. Next, the cell membrane was stained with WGA Alexa Fluor® 488 conjugate according to the provider. Briefly, a stock solution of 1 mg/mL of the conjugate was prepared using PBS and used to make up enough staining solution to cover the cells by diluting it at a concentration of 5 μg/mL using sterile PBS. The cells were incubated for 10 min at 37 °C with the conjugate solution and washed twice with sterile PBS. The cells were fixed using paraformaldehyde as follows: freshly prepared 4 % PFA in PBS was added to fully cover the slides. The cells were then incubated at room temperature for 15 min, followed by three washes with PBS. Finally, the coverslips were mounted on microscope slides using ProLong Gold (containing DAPI for nucleus staining). Finally, the slides were left to dry for 24 h at 37 °C with 5 % $CO_2$. The confocal images were taken using the confocal laser scanning microscope Nikon A1R using 400x magnification.

### 5.7. Flow cytometry to measure vesicle affinity to cell lines

6 well plates were seeded with 1 mL of either HFFF, HEK293, or HEPG2 at a $3x10^5$ cells/mL density. The plate was incubated for 48 h at 37 °C with 5 % $CO_2$. After incubation, the media was replaced with 1 mL of vesicle solution at a concentration of 100 mM. The plate was returned to the incubator for 4 h. After incubation with the vesicle solutions, the cells were carefully washed three times with PBS, and the cellular membrane was stained using 5 μg/mL WGA as described in the previous section. After staining, the cells were trypsinised, washed and resuspended in 1 mL of FACS buffer (PBS + 5 % FBS) and strained through a 40 μm sieve. (Flowmi cell strainers, SP Bel-Art, Wayne, United States). The cells were analysed using a CytoFLEX LX (Beckman Coulter) with CytExpert software (version 2.6). The gating strategy is shown in Fig. 3. 10,000 events in the rhodamine-positive gatewere recorded, and the analysis of fluorescence intensity was carried out using the FlowJo 10.8.1 software (Becton, Dickinson & Company)

### 5.8. TNF-α quantification

TNF-α quantification used an R&D systems kit (DTA00D) on the cell supernatant: two plates were seeded with HFFF2 at $3x10^5$ cells/mL concentration and incubated for 48 h at 37 °C with 5 % $CO_2$. Subsequently, the cells were exposed to 1 mL of vesicle solutions at a 100 μM concentration (diluted in uncompleted DMEM media) and returned to the incubator. As a positive control, the cells were exposed to 10 μg/mL *E. coli* LPS and complete DMEM media was used as negative control; one well plate was incubated for 4 h and a second one for 24 h. After each time point, the supernatant was retrieved from the well plates, centrifugated at 100 g for 5 min to remove debris and used in the assay according to the manufacturer (R&D systems). Briefly, 50 μL of assay diluent RD1F was added to each well of the provided 96-well plate, 50 μL of standards, control or sample per well were added and incubated for 2 h at room temperature on a microplate shaker (500 ± 50 rpm). The contents of the plate were aspirated and washed four times with wash buffer. After the last wash, the liquid was entirely removed by inversion and blotting the plate against clean paper towels. 200 μL of Human TNF-α conjugate was added to each well, incubated and washed just as previously described. 200 μL of substrate solution was added to each well and incubated on the benchtop protected from light. Finally, 50 μL of a stop solution was added to each well and gently mixed by hand to ensure thorough mixing. The plate was read within 30 min using a microplate reader at 450 nm.

### 5.9. Statistical analysis

Each experiment was performed in three independent repeats and given as the mean ± standard deviation. The results were analysed for statistically significant differences using a one-way ANOVA, followed by Tukey's multiple comparisons or Dunnett's test post hoc test as indicated.

## Author contributions

All authors conceptualised the present research. JM, NI, PB, and DJ developed the methodology. JM investigated and performed experiments and data collection. JM, PB, and NI performed a formal analysis of the data. JM prepared the initial draft. All authors contributed to the review and editing of the first draft. PB, DJ, and NK oversaw and led the research. JM, PB, and DJ acquired financial support for the project, which led to this manuscript.

## CRediT authorship contribution statement

**Juan Martinez:** Writing – original draft, Methodology, Investigation, Formal analysis, Data curation. **Nicola Ingram:** Writing – review & editing, Supervision, Methodology, Investigation, Formal analysis. **Nikil Kapur:** Writing – review & editing, Supervision, Investigation, Formal analysis, Conceptualization. **David G. Jayne:** Writing – review & editing, Supervision, Project administration, Methodology, Investigation, Funding acquisition, Formal analysis, Conceptualization. **Paul A. Beales:** Writing – review & editing, Supervision, Project administration, Methodology, Investigation, Funding acquisition, Formal analysis, Conceptualization.

## Declaration of competing interest

The authors declare that they have no known competing financial interests or personal relationships that could have appeared to influence the work reported in this paper.

## Acknowledgements

J.M. thanks CONACYT for funding through a PhD scholarship (CVU-818948). The authors also acknowledge funding from Leeds Hospitals Charity and the University of Leeds Impact Acceleration Account (WT iTPA) [219420/Z/19/Z]. NI was funded by EPSRC (EP/P023266/1) and is currently supported by the National Institute for Health and Care Research (NIHR) Leeds Biomedical Research Centre (BRC) (NIHR203331). The views expressed are those of the author(s) and not necessarily those of the NHS, the NIHR or the Department of Health and Social Care.

## Appendix A. Supplementary data

Supplementary data to this article can be found online at https://doi.org/10.1016/j.jcis.2025.137664.

## Data availability

Data will be made available on request.

## References

[1] V.P. Torchilin, Recent advances with liposomes as pharmaceutical carriers, Nat. Rev. Drug Discov. 4 (2) (2005) 145–160.
[2] T.M. Allen, P.R. Cullis, Liposomal drug delivery systems: from concept to clinical applications, Adv Drug Deliv Rev 65 (1) (2013) 36–48.
[3] P. Liu, G. Chen, J. Zhang, A Review of Liposomes as a Drug Delivery System: Current Status of Approved Products, Regulatory Environments, and Future Perspectives, Molecules 27 (4) (2022).
[4] E. Rideau, R. Dimova, P. Schwille, F.R. Wurm, K. Landfester, Liposomes and polymersomes: a comparative review towards cell mimicking, Chem. Soc. Rev. 47 (23) (2018) 8572–8610.
[5] N. Habibi, N. Kamaly, A. Memic, H. Shafiee, Self-assembled peptide-based nanostructures: Smart nanomaterials toward targeted drug delivery, Nano Today 11 (1) (2016) 41–60.
[6] N.A.C. Jackson, K.E. Kester, D. Casimiro, S. Gurunathan, F. DeRosa, The promise of mRNA vaccines: a biotech and industrial perspective, npj Vaccines 5 (1) (2020) 11.
[7] P. Foroozandeh, A.A. Aziz, Insight into Cellular Uptake and Intracellular Trafficking of Nanoparticles, Nanoscale Res Lett 13 (1) (2018) 339.
[8] P.L. Felgner, T.R. Gadek, M. Holm, R. Roman, H.W. Chan, M. Wenz, J.P. Northrop, G.M. Ringold, M. Danielsen, Lipofection: a highly efficient, lipid-mediated DNA-transfection procedure, Proc Natl Acad Sci U S A 84 (21) (1987) 7413–7417.
[9] K.A. Dawson, A. Salvati, I. Lynch, Nanotoxicology: Nanoparticles reconstruct lipids, Nat. Nanotechnol. 4 (2) (2009) 84–85.
[10] S. Takano, Y. Aramaki, S. Tsuchiya, Physicochemical properties of liposomes affecting apoptosis induced by cationic liposomes in macrophages, Pharm Res 20 (7) (2003) 962–968.
[11] H. Lv, S. Zhang, B. Wang, S. Cui, J. Yan, Toxicity of cationic lipids and cationic polymers in gene delivery, J Control Release 114 (1) (2006) 100–109.
[12] T. Shehata, K. Ogawara, K. Higaki, T. Kimura, Prolongation of residence time of liposome by surface-modification with mixture of hydrophilic polymers, Int J Pharm 359 (1–2) (2008) 272–279.
[13] C. Weber, M. Voigt, J. Simon, A.K. Danner, H. Frey, V. Mailänder, M. Helm, S. Morsbach, K. Landfester, Functionalization of Liposomes with Hydrophilic Polymers Results in Macrophage Uptake Independent of the Protein Corona, Biomacromolecules 20 (8) (2019) 2989–2999.
[14] T.M. Allen, C. Hansen, F. Martin, C. Redemann, A. Yau-Young, Liposomes containing synthetic lipid derivatives of poly(ethylene glycol) show prolonged circulation half-lives in vivo, Biochim. Biophys. Acta 1066 (1) (1991) 29–36.
[15] S. Priya, V.M. Desai, G. Singhvi, Surface Modification of Lipid-Based Nanocarriers: A Potential Approach to Enhance Targeted Drug Delivery, ACS Omega 8 (1) (2023) 74–86.
[16] J.M. Harris, R.B. Chess, Effect of pegylation on pharmaceuticals, Nat. Rev. Drug Discov. 2 (3) (2003) 214–221.
[17] Y. Ju, J.M. Carreño, V. Simon, K. Dawson, F. Krammer, S.J. Kent, Impact of anti-PEG antibodies induced by SARS-CoV-2 mRNA vaccines, Nat. Rev. Immunol. 23 (3) (2023) 135–136.
[18] Y.K. Go, C. Leal, Polymer–Lipid Hybrid Materials, Chem. Rev. 121 (22) (2021) 13996–14030.
[19] J.F. Le Meins, C. Schatz, S. Lecommandoux, O. Sandre, Hybrid polymer/lipid vesicles: state of the art and future perspectives, Mater. Today 16 (10) (2013) 397–402.
[20] E. Brodszkij, B. Städler, Advances in block copolymer-phospholipid hybrid vesicles: from physical–chemical properties to applications, Chem. Sci. 15 (28) (2024) 10724–10744.
[21] N. Pippa, E. Kaditi, S. Pispas, C. Demetzos, PEO-b-PCL–DPPC chimeric nanocarriers: self-assembly aspects in aqueous and biological media and drug incorporation, Soft Matter 9 (15) (2013) 4073–4082.
[22] S. Khan, J. McCabe, K. Hill, P.A. Beales, Biodegradable hybrid block copolymer – lipid vesicles as potential drug delivery systems, J. Colloid Interface Sci. 562 (2020) 418–428.
[23] R. Seneviratne, L.J.C. Jeuken, M. Rappolt, P.A. Beales, Hybrid Vesicle Stability under Sterilisation and Preservation Processes Used in the Manufacture of Medicinal Formulations, Polymers (2020).
[24] M. Tuteja, M. Kang, C. Leal, A. Centrone, Nanoscale partitioning of paclitaxel in hybrid lipid–polymer membranes, Analyst 143 (16) (2018) 3808–3813.
[25] M. Kang, B. Lee, C. Leal, Three-Dimensional Microphase Separation and Synergistic Permeability in Stacked Lipid–Polymer Hybrid Membranes, Chem. Mater. 29 (21) (2017) 9120–9132.
[26] N. Kambar, C. Leal, Microfluidic synthesis of multilayered lipid–polymer hybrid nanoparticles for the formulation of low solubility drugs, Soft Matter 19 (8) (2023) 1596–1605.
[27] W. Zong, B. Thingholm, F. Itel, P.S. Schattling, E. Brodszkij, D. Mayer, S. Stenger, K.N. Goldie, X. Han, B. Städler, Phospholipid–Block Copolymer Hybrid Vesicles with Lysosomal Escape Ability, Langmuir 34 (23) (2018) 6874–6886.
[28] Y. Zhang, N. Gal, F. Itel, I.N. Westensee, E. Brodszkij, D. Mayer, S. Stenger, M. Castellote-Borrell, T. Boesen, S.R. Tabaei, F. Höök, B. Städler, Hybrid vesicles as intracellular reactive oxygen species and nitric oxide generators, Nanoscale 11 (24) (2019) 11530–11541.
[29] E. Brodszkij, I.N. Westensee, M. Bertelsen, N. Gal, T. Boesen, B. Städler, Polymer–Lipid Hybrid Vesicles and Their Interaction with HepG2 Cells, Small 16 (27) (2020) 1906493.
[30] P. De Dios Andres, I.N. Westensee, E. Brodszkij, M.A. Ramos-Docampo, N. Gal, B. Städler, Evaluation of Hybrid Vesicles in an Intestinal Cell Model Based on Structured Paper Chips, Biomacromolecules 22 (9) (2021) 3860–3872.
[31] C. Ade, X. Qian, E. Brodszkij, P. De Dios Andres, J. Spanjers, I.N. Westensee, B. Städler, Polymer Micelles vs Polymer–Lipid Hybrid Vesicles: A Comparison Using RAW 264.7 Cells, Biomacromolecules 23 (3) (2022) 1052–1064.
[32] Z. Cheng, D.R. Elias, N.P. Kamat, E.D. Johnston, A. Poloukhtine, V. Popik, D. A. Hammer, A. Tsourkas, Improved Tumor Targeting of Polymer-Based Nanovesicles Using Polymer–Lipid Blends, Bioconjug. Chem. 22 (10) (2011) 2021–2029.
[33] J. Nam, T.K. Vanderlick, P.A. Beales, Formation and dissolution of phospholipid domains with varying textures in hybrid lipo-polymersomes, Soft Matter 8 (30) (2012) 7982–7988.
[34] S.K. Lim, H.-P. De Hoog, A.N. Parikh, M. Nallani, B. Liedberg, Hybrid, Nanoscale Phospholipid/Block Copolymer Vesicles, Polymers 5 (3) (2013) 1102–1114.
[35] R. Seneviratne, R. Catania, M. Rappolt, L.J.C. Jeuken, P.A. Beales, Membrane mixing and dynamics in hybrid POPC/poly(1,2-butadiene-block-ethylene oxide) (PBd-b-PEO) lipid/block co-polymer giant vesicles, Soft Matter 18 (6) (2022) 1294–1301.
[36] R. Seneviratne, G. Coates, Z. Xu, C.E. Cornell, R.F. Thompson, A. Sadeghpour, D. P. Maskell, L.J.C. Jeuken, M. Rappolt, P.A. Beales, High Resolution Membrane Structures within Hybrid Lipid-Polymer Vesicles Revealed by Combining X-Ray Scattering and Electron Microscopy, Small 19 (22) (2023) e2206267.
[37] R. Seneviratne, L.J.C. Jeuken, M. Rappolt, P.A. Beales, Hybrid vesicle stability under sterilisation and preservation processes used in the manufacture of medicinal formulations, Polymers 12 (4) (2020).
[38] D.E. Owens 3rd, N.A. Peppas, Opsonization, biodistribution, and pharmacokinetics of polymeric nanoparticles, Int J Pharm 307 (1) (2006) 93–102.
[39] E.H. Shin, Y. Li, U. Kumar, H.V. Sureka, X. Zhang, C.K. Payne, Membrane potential mediates the cellular binding of nanoparticles, Nanoscale 5 (13) (2013) 5879–5886.
[40] Atcc, Hep G2 [HEPG2], 2022.
[41] Atcc, 293 [HEK-293], 2022.
[42] S.P. Samuel, N. Jain, F. O'Dowd, T. Paul, D. Kashanin, V.A. Gerard, Y.K. Gun'ko, A. Prina-Mello, Y. Volkov, Multifactorial determinants that govern nanoparticle

uptake by human endothelial cells under flow, Int J Nanomedicine 7 (2012) 2943–2956.
[43] S. Shurbaji, G.A. G, A.H. E, A. Elzatahry, C.Y. H, Effect of Flow-Induced Shear Stress in Nanomaterial Uptake by Cells: Focus on Targeted Anti-Cancer Therapy, Cancers (Basel) 12(7) (2020).
[44] T. Kang, C. Park, J.-S. Choi, J.-H. Cui, B.-J. Lee, Effects of shear stress on the cellular distribution of polystyrene nanoparticles in a biomimetic microfluidic system, J. Drug Delivery Sci. Technol. 31 (2016) 130–136.
[45] Ibidi, Shear stress and shear rates for ibidi microslides- Based on numerical calculations, Version 4,1 (March 2016) (2016) 16-16.
[46] J.K. Kular, S. Basu, R.I. Sharma, The extracellular matrix: Structure, composition, age-related differences, tools for analysis and applications for tissue engineering, 2014.
[47] N.S. Heaton, G. Randall, Multifaceted roles for lipids in viral infection, Trends Microbiol. 19 (7) (2011) 368–375.
[48] K. Simons, J.L. Sampaio, Membrane organization and lipid rafts, Cold Spring Harb. Perspect. Biol. 3 (10) (2011) a004697.
[49] A. Albanese, P.S. Tang, W.C.W. Chan, The Effect of Nanoparticle Size, Shape, and Surface Chemistry on Biological Systems, Annual Review of Biomedical Engineering 14(Volume 14, 2012) (2012) 1-16.
[50] J.F. Le Meins, C. Schatz, S. Lecommandoux, O. Sandre, Hybrid polymer/lipid vesicles. State of the Art and Future Perspectives, 2013.
[51] N. Kučerka, M.P. Nieh, J. Katsaras, Fluid phase lipid areas and bilayer thicknesses of commonly used phosphatidylcholines as a function of temperature, Biochim. Biophys. Acta Biomembr. (2011).
[52] D. Peer, J.M. Karp, S. Hong, O.C. Farokhzad, R. Margalit, R. Langer, Nanocarriers as an emerging platform for cancer therapy, Nat. Nanotechnol. 2 (12) (2007) 751–760.
[53] J. Ismail, L.C. Klepsch, P. Dahlke, E. Tsarenko, A. Vollrath, D. Pretzel, P.M. Jordan, K. Rezaei, J.A. Czaplewska, S. Stumpf, B. Beringer-Siemers, I. Nischang, S. Hoeppener, O. Werz, U.S. Schubert, PEG-Lipid-PLGA Hybrid Particles for Targeted Delivery of Anti-Inflammatory Drugs, Pharmaceutics 16 (2) (2024).
[54] S. Raffy, J. Teissié, Control of Lipid Membrane Stability by Cholesterol Content, Biophys. J . 76 (4) (1999) 2072–2080.
[55] C.R. Bertozzi, L.L. Kiessling, Chemical glycobiology, Science 291 (5512) (2001) 2357–2364.
[56] B. Yue, Biology of the extracellular matrix: an overview, Journal of Glaucoma 23 (1536-481X (electronic)) (2014) S20–S23.
[57] C. Liu, L. Zhang, W. Zhu, R. Guo, H. Sun, X. Chen, N. Deng, Barriers and Strategies of Cationic Liposomes for Cancer Gene Therapy, Mol Ther Methods Clin Dev 18 (2020) 751–764.
[58] C. Lonez, M. Vandenbranden, J.-M. Ruysschaert, Cationic liposomal lipids: From gene carriers to cell signaling, Prog. Lipid Res. 47 (5) (2008) 340–347.
[59] R. Kolašinac, C. Kleusch, T. Braun, R. Merkel, A. Csiszár, Deciphering the Functional Composition of Fusogenic Liposomes, Int. J. Mol. Sci. 19 (2) (2018) 346.
[60] C. Bellefroid, C. Reusch, A. Lechanteur, B. Evrard, F. Debacq-Chainiaux, D. Mottet, G. Piel, Systematic study of liposomes composition towards efficient delivery of plasmid DNA as potential application of dermal fibroblasts targeting, Int. J. Pharm. 593 (2021) 120122.
[61] V. De Leo, F. Milano, A. Agostiano, L. Catucci, Recent Advancements in Polymer/Liposome Assembly for Drug Delivery: From Surface Modifications to Hybrid Vesicles, Polymers (basel) 13 (7) (2021).
[62] S. Hua, S.Y. Wu, The use of lipid-based nanocarriers for targeted pain therapies, Front Pharmacol 4 (2013) 143.
[63] D.C. Fernandes, T.L.S. Araujo, F.R.M. Laurindo, L.Y. Tanaka, Hemodynamic Forces in the Endothelium: From Mechanotransduction to Implications on Development of Atherosclerosis, 2018.
[64] S. Fontenete, D. Carvalho, A. Lourenço, N. Guimarães, P. Madureira, C. Figueiredo, N.F. Azevedo, FISHji: New ImageJ macros for the quantification of fluorescence in epifluorescence images, Biochem. Eng. J. 112 (2016) 61–69.